



AIAA 95-2615

**Assessment of Turbulence Models in
Overexpanded 2D-CD Nozzle Flow Simulations**

A. Hamed and C. Vogiatzis

University of Cincinnati

Cincinnati, OH

**31st AIAA/ASME/SAE/ASEE
Joint Propulsion Conference and Exhibit
July 10-12, 1995/San Diego, CA**

ASSESSMENT OF TURBULENCE MODELS IN OVEREXPANDED 2D-CD NOZZLE FLOW SIMULATIONS

A. Hamed* and C. Vogiatzis**
University of Cincinnati
Cincinnati, OH 45221

Abstract

An investigation was conducted to assess the performance of different turbulence models in the numerical simulations of two dimensional convergent divergent (2DCD) nozzle flow fields at overexpanded conditions. The implicit numerical solution of the compressible two dimensional Navier-Stoke equations was obtained using the NPARC code. Five different turbulence closure models were used in the computations and the results compared to existing experimental data at design and overexpanded conditions. The results indicate little differences among the predictions using the algebraic, one equation, and two equation turbulence models at design pressure ratio. However large differences in the predicted shock location and pressure level behind the shock were observed at overexpanded conditions. The two equation $k-\epsilon$ and $k-\omega$ turbulence models, gave the best overall agreement with the experimental measurements for thrust and static pressure distribution over the flaps. The agreement deteriorates with decreased nozzle pressure ratio (NPR) as the shock moves upstream and three dimensional flow effects increase downstream.

Introduction

There is renewed interest in 2D-CD nozzles because of the advantages they offer over axisymmetric configurations for supersonic transport. These include higher performance, reduced afterbody drag, easier integration with airframes, and large mechanical area excursion capabilities. It is well known that the take off gross weight is very sensitive to nozzle performance at cruise flight conditions¹, and that high area ratios are required for best efficiency at supersonic cruise. The performance of these nozzles can suffer at off design conditions when the large nozzle area ratio reductions required during subsonic and transonic acceleration, cannot be achieved under the mechanical and control system constraints. Since this can adversely affect the acceleration time to cruise, the fuel burnt and range, it is desirable to predict off design performance with a high degree of accuracy.

Very few experimental studies report detailed measurements in overexpanded 2D-CD nozzles. Mason et al² presented internal performance data for five 2D-CD nozzle geometries tested in the static test facility of Langley's 16-ft transonic tunnel. Hunter³ tested another 2D-CD nozzle configuration in the same facility and reported experimental data for the internal thrust and discharge coefficients, and static pressure distribution over the flap at different NPRs.

Overexpanded nozzle predictions are complicated by the large shock induced separated flow regions in the divergent nozzle section. Gerard et al⁴ and Shieh⁵ presented computational results at one overexpanded condition, and compared only the static pressure distribution with the experimental data of Mason et al². Hamed et al⁶ presented computational results at several overexpanded flow conditions for two 2D-CD nozzle configurations tested by Mason² and Hunter³. They also modeled the interactions with the external flow by extending the solution domain outside the nozzle. The purpose of the present investigation is to assess the computational results obtained using five different turbulence models in terms of the convergence characteristics and the agreement of the computed pressure distribution and thrust coefficient with the experimental data in overexpanded 2D-CD nozzles.

2D-CD nozzle. Configuration and operating conditions.

The 2D-CD nozzle tested by Hunter³ in Langley's static test facility was selected for the numerical assessment because the large number of pressure taps gave a better definition of the shock location. The nozzle has a design pressure ratio of 8.8 for an exit Mach number of 2.1. The convergent nozzle section's area ratio is 2.56 and its convergence angle 22.3°, while the divergent nozzle section's area ratio is 1.796 and its divergence angle 11.2°. The distance between the side walls is approximately 4.1 times the throat height of 1.08 inches, and the throat radius of curvature is $r_c=0.625$ inches. The nozzle was tested at design and several overexpanded flow conditions for NPR's ranging between 1.255 and 8.8. The experimental results³ consist of flow and thrust

*Professor, Fellow AIAA

** Student Member AIAA

coefficients, as well as static pressure distribution over the flaps at the centerline, and at 10% of the nozzle width from the endwalls. In addition Schlieren photographs were also presented showing the location and structure of the shock in the divergent nozzle section.

Computations

Flow Solver and Boundary Conditions

The NPARC code was used to obtain the numerical solution to the compressible two dimensional Navier-Stokes equations on Cray Y-MP. The code is based on the use of the approximate factorization scheme of Beam-Warming in the solution of the time dependent, Reynolds averaged Navier-Stokes equations in conservation law form and general curvilinear coordinates. The computations were performed using five different turbulence models, namely Baldwin-Lomax and RNG algebraic models, Baldwin-Barth one equation model, and the two equation $k-\epsilon$ and $k-\omega$ turbulence models of Chien⁸ and Wilcox⁹ respectively. The first four turbulence models exist in NPARC-2.0. The last was implemented in NPARC-2.1 by Yoder and Georgiadis¹⁰. The flow is computed in the lower half of the nozzle, with symmetry boundary conditions at the upper boundary, and no slip adiabatic boundary conditions over the flap. Free boundary conditions were applied at the nozzle inlet and exit.

Computational Grid

Referring to figure 1, a one block 161x68 grid, was generated in the lower half of the nozzle using an elliptic grid generator (GRIDGEN¹¹), with half the grid points in the divergent part of the nozzle. The Y^+ for the first grid point next to the wall was equal to 1.0 in the throat region, with at least 15 points inside the wall boundary layer.

This grid was selected after a grid refinement study was conducted at 2.41 nozzle pressure ratio. The results obtained using the 161x68 grid of figure 1 and a coarser (81x34) with the same value of Y^+ for the first grid from the nozzle wall, were very close in predicting the pressure distribution before and after the shock, and differed only in the pressure gradient across the shock, which improved with grid refinement.

Convergence

The solution was advanced using local time stepping and the maximum allowable CFL value. This varied from 2.0 for the high pressure ratio cases to 1.0-1.5 for the low pressure ratios. The nozzle thrust and flow coefficients were computed and monitored during the iterations. The internal thrust coefficient was determined from the integration of the axial momentum at the exit plane, and the flow coefficient, from the integration of the mass flux at several normal planes upstream of the throat. A variation of less than 0.1% in thrust or mass flow over 1000 iterations was required, to consider the solution converged. Additional iterations were sometimes required to converge the nozzle performance parameters, after the residual information indicated convergence, typically 2 to 4 orders of magnitude reduction. Conversely small flow regions sometimes kept the numerical residuals from further reductions after the nozzle performance parameters have converged. Weterlen et al¹² reported similar behavior in their numerical computations of nozzle drag.

Results And Discussions

Computational results are presented and compared with the experimental data of Hunter³ over a range of nozzle pressure ratios corresponding to design and several overexpanded conditions.

Predictions at the design pressure ratio

The convergence characteristics of the numerical solution obtained using the different turbulence models at design pressure ratio are shown in figure 2. In all cases the numerical solution was advanced using local time stepping from uniform initial conditions corresponding to one dimensional subsonic flow at the nozzle inlet. The maximum CFL number for these cases was found to be equal to 2.0. The algebraic turbulence models were used from the beginning of the calculation. For the one and two equation models, the turbulence viscosity field was initialized using Baldwin-Lomax turbulence model for 2000 iterations. According to figure 2 the residuals are reduced three orders of magnitude within 5,000 iterations and another order of magnitude over the next 5,000 iterations in all cases but the RNG turbulence model, where it does not decrease below two orders of magnitude.

The computed pressure distributions for the different turbulence models are shown in figure 3. The

curves practically coincide and the agreement with the experiment is excellent. A comparison of the computed nozzle performance predictions for the five turbulence models at design conditions is summarized in table 1. According to this data, the thrust coefficient was predicted within 0.8% of the experimental results in all cases except for the RNG model where the predictions were within 1.0%.

Predictions at overexpanded conditions

The computations of the nozzle flow field were performed using the five turbulence models at one overexpanded condition corresponding to a nozzle pressure ratio 2.41 (27% of design value). From the convergence history shown in figure 4, it is obvious that the total residual decrease is approximately two orders of magnitude smaller than the design pressure ratio case. This is attributed to the massive shock induced flow separation, which occupies over 60% of the divergent nozzle length and 30 % of the exit width. The typical thrust coefficient evolution presented in figure 5 indicates that variation of less than 0.1% are reached after 10,000 iterations.

Typical Mach number and turbulence viscosity contours and velocity vectors, are presented in figures 7a, 7b and 7c. These results, which were obtained using the $k-\omega$ model, indicate a normal shock with a large well defined lambda foot. The leading branch of the lambda shock extends to the nozzle surface, where the flow separates and remains detached to the nozzle exit. The highest turbulence viscosity levels are predicted in the separated flow region behind the shock.

The surface pressure distributions shown in figure 7 indicate that there is a significant spread, of about 40% of the throat opening in the predicted shock location, depending on the turbulence model used.. At this pressure ratio Wilcox's $k-\omega$ model was the closest to the experimental results in predicting the pressure variation behind the shock, but Chien's $k-\epsilon$ model was closer in predicting the shock location. The algebraic and one equation models predicted shock positions respectively upstream and downstream of the experimental location. Furthermore, their predicted post shock pressures were higher, and contained overshoots not observed experimentally.

The computed exit velocity profiles using the different turbulence models are compared in figure 8. The results indicate that the shear layer is independent

of the turbulence model in spite of the difference in the predicted shock location. The predictions using the one equation turbulence model of Baldwin-Barth exhibited the largest velocities in the supersonic region above, and the reversed flow region below the shear layer. Conversely the predictions using the algebraic turbulence models exhibited the lowest velocities in both these regions. The predicted velocities were very close in the core transonic region, with the highest values predicted by the $k-\omega$ model and the lowest by the algebraic models.

The corresponding thrust coefficients are compared with the experimental results in table 2. The computed thrust coefficients using all the turbulence models with the exception of Baldwin-Lomax are higher than the experimental value. Despite the fact that the pressure distribution predicted using the algebraic turbulence models (Baldwin-Lomax and RNG) exhibited the largest deviation from the experimental results, the thrust coefficients predicted by these models are fortuitously closest to the experimental value.

Further numerical solutions were obtained with the two equation turbulence models over a number of overexpanded pressure ratios. Figure 9 and figure 10 compare the computed static pressure distribution over the flap to the experimental results of Hunter³ at the centerline and near the end walls. Satisfactory agreement with the experimental results is observed at nozzle pressure ratios above 2.41. The three dimensional effects downstream of the shock increase below this pressure ratio as indicated by the differences between the static pressure at the centerline and the flap end wall. Table 3 and figure 11 compare the computed thrust coefficient using the two equation turbulence models, with the experimental results at five different nozzle pressure ratios. The two equation turbulence model thrust coefficient predictions are within 1% of the experimental data for nozzle pressure ratios above 50% design, and within 2% above 30% design. Increased deviations at lower pressure ratios are attributed to three dimensional flow effects caused by the interactions between the shock and endwall boundary layers.

Conclusions

An assessment of five turbulence models was conducted in a 2DCD nozzle at different operating conditions. The two dimensional flow field solutions using the NPARC code were required to meet several

convergence criteria including the nozzle flow and thrust coefficients. The turbulence models considered are the algebraic models of Baldwin-Lomax, RNG, the one equation model of Baldwin-Barth and the two equation $k-\epsilon$ and $k-\omega$ models of Chien and Wilcox. All five turbulence models yielded essentially identical solutions at design points and correlated well with the experimental pressure distribution over the flaps. The internal thrust coefficient predictions were within 0.8% of the experimental data under these conditions in all cases but the RNG model.

At overexpanded conditions agreements among the different models and with the experimental data prevailed only up to the point of shock induced flow separation and then varied significantly in the predicted shock location and pressure level behind the shock. The algebraic turbulence models predicted the shock location downstream of the experimental position, and the one equation model predicted the shock location upstream of the experimental position. Both overpredicted the pressure level behind the shock with overshoots not exhibited in the experimental pressure distribution. The two equation turbulence models gave the best Overall agreement with the experimental pressure distributions at overexpanded conditions. In spite of the massive flow separation, the thrust coefficient was predicted within 1.0% of the experimental values for nozzle pressure ratios above 50% design. Below these pressures, two dimensional flow predictions are inadequate because of the strong three dimensional flow effects behind the shock.

Acknowledgment

This work was sponsored by Ohio Aerospace Institute Subgrant No. 120520. The computational work was performed on the CRAY YMP of the Ohio Supercomputer Center

References

¹ Shaw, R. J., Gilkey, S. and Hines, R., "Engine Technology Challenges for 21st Century High Speed Civil Transport" International Symposium on Air Breathing Engines, Tokyo, Japan, Sept. 20-24, 1993.

² Mason, M.L., Putnam, L.E., and Re, R.J., "The Effect of Throat Contouring on Two-Dimensional Converging-Diverging Nozzles at Static Conditions." NASA TP 1704, August, 1980.

³ Hunter, C.A., "An Experimental Analysis of Passive Shock-Boundary Layer Interaction Control for Improving the Off-Design Performance of Jet Exhaust Nozzles, M.S. Thesis, George Washington Univ., September 1993.

⁴ Garrard, G., Phares W., Cooper G., "Calibration Of Parc for Propulsion Flows", AIAA/SAE/ASME/ASEE 27th Joint Propulsion Conference, June 24-26, 1991, Sacramento, CA

⁵ Shieh, Fang Shih, "Navier-Stokes Solutions of Transonic Nozzle Flow with Shock Induced Flow Separations," Journal of Propulsion and Power, Vol. 8, No. 4, July-August 1992, pp. 829-835

⁶ Hamed A., Vogiatzis C., Yeuan J.J., "Performance Prediction of Overexpanded 2D-CD Nozzles", 12th International Symposium on Air Breathing Engines, September 10-15, 1995, Melbourne, Australia

⁷ Cooper, G.K. and Sirbaugh, J.R., "PARC Code: Theory and Usage," AEDC-TR-89-15, 1989.

⁸ Chien, K-Y, "Prediction of Channel and Boundary-Layer Flows with a Low Reynolds Number Turbulence Model," AIAA Journal, Vol. 20, January 1982, pp. 33-38.

⁹ Wilcox, D.D., "The Remarkable Ability of Turbulence Model Equations to Describe Transition", Fifth Symposium on Numerical and Physical Aspects of Aerodynamic Flows, California State University, Long Beach, California, 13-15 January 1992.

¹⁰ Yoder, D.A., Georgiadis N.J., "A User's Guide to NPARC k-w", Private Communication.

¹¹ Steinbrenner, J.P., Chawner, J.R., and Fouts, C.L., "The GRIDGEN 3D Multiple Block Grid Generation System", WRDC-TR-90-3022 Vols. I and II, Wright-Patterson AFB, OH, 1990

¹² Welterlen, T.J., Catt, J.A. and Reno, J.M., "Evaluating F-16 Nozzle Drag Using Computational Fluid Dynamics" AIAA 94-0022, Jan 1994.

	Experiment	Wilcox k- ω	Chien k- ϵ	Baldwin-Barth	Baldwin-Lomax	RNG
Thrust Coefficient	0.987	0.995	0.995	0.995	0.995	0.997
%error in thrust	-	0.8%	0.8%	0.8%	0.8%	1.0%

Table 1. Thrust coefficient at design pressure ratio (NPR=8.81).

	Experiment	Wilcox k- ω	Chien k- ϵ	Baldwin-Barth	Baldwin-Lomax	RNG
Thrust Coefficient	0.904	0.923	0.927	0.941	0.898	0.907
%error in thrust		2.1%	2.5%	4.1%	-0.7%	0.3%

Table 2. Thrust coefficient at NPR=2.41 (27% of design pressure ratio).

		NPR=2.0	NPR=2.4	NPR=3.4	NPR=4.6	NPR=8.8
Experiment		0.866	0.904	0.935	0.959	0.987
k- ϵ	Thrust Coefficient	0.900	0.927	0.947	0.966	0.995
	%error in thrust	3.9%	2.5%	1.3%	0.7%	0.8%
k- ω	Thrust Coefficient	0.911	0.923	0.952	0.971	0.995
	%error in thrust	5.2%	2.1%	1.8%	1.2%	0.8%

Table 3. Thrust coefficient at different pressure ratios

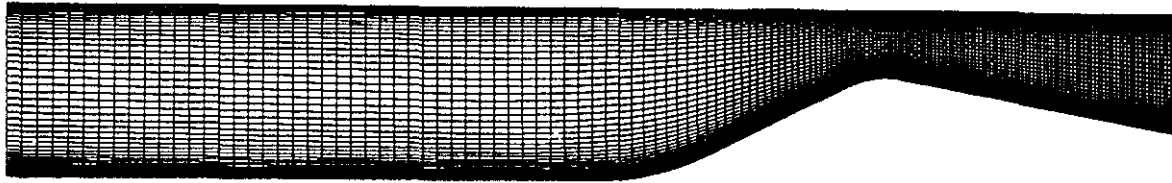


Figure 1. Computational grid (161x68).

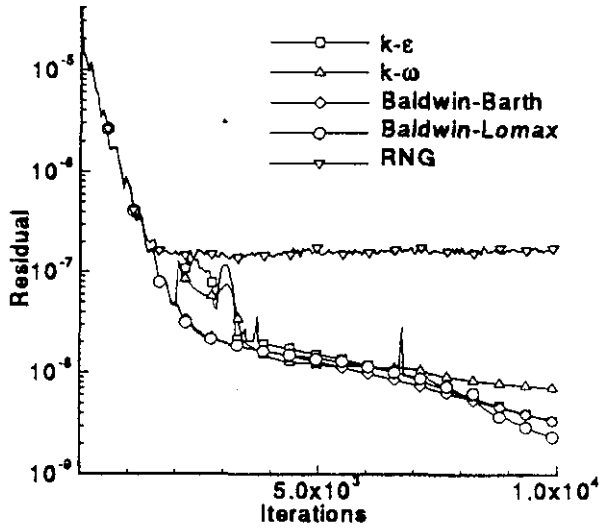


Figure 2. Convergence history at design pressure ratio (NPR=8.8).

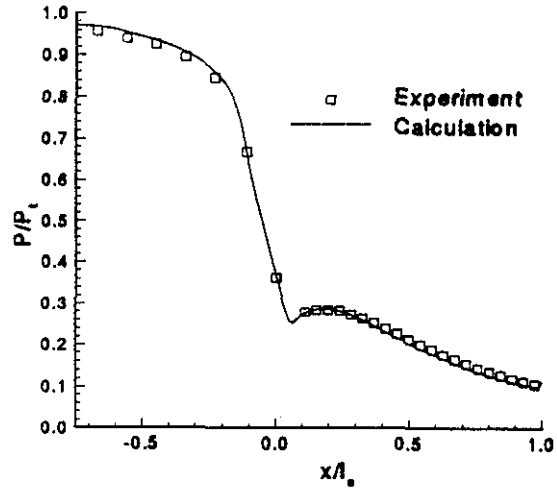


Figure 3. Surface pressure distribution at design pressure ratio (NPR=8.8).

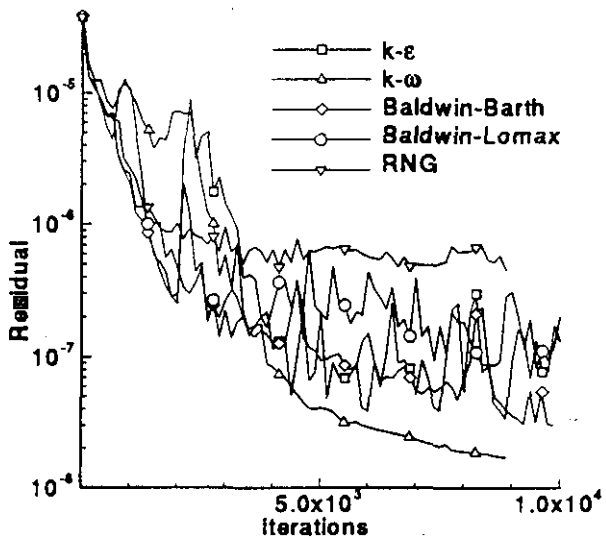


Figure 4. Convergence history (NPR=2.41)

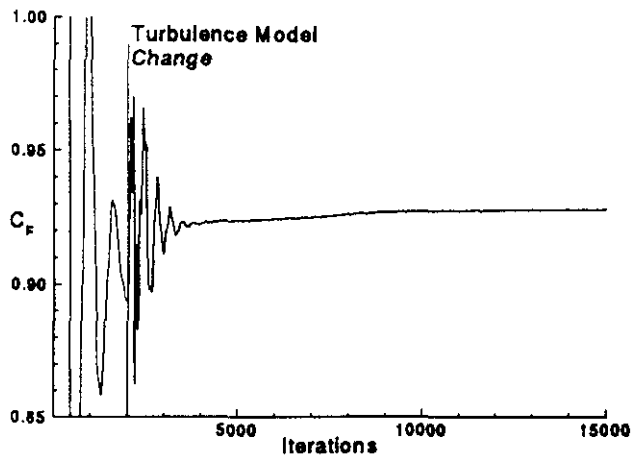


Figure 5. Thrust coefficient evolution (NPR=2.41).

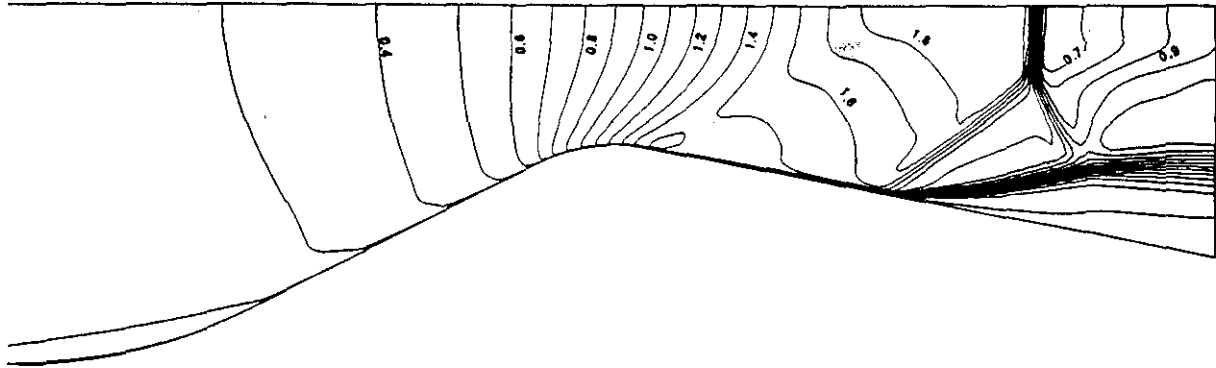


Figure 6a. Mach number contours using the $k-\omega$ turbulence model (NPR=2.41)

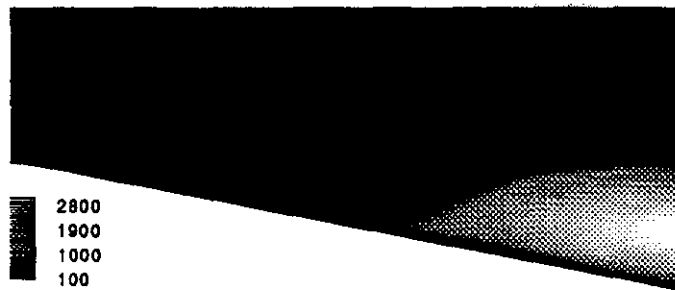


Figure 6b. Turbulence viscosity contours using the $k-\omega$ turbulence model (NPR=2.41)

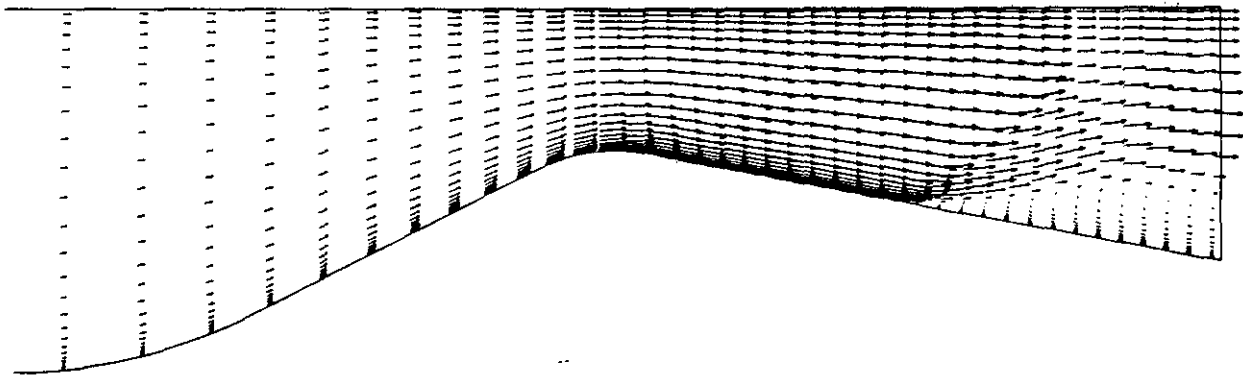


Figure 6c Velocity vectors using the $k-\omega$ turbulence model (NPR=2.41)

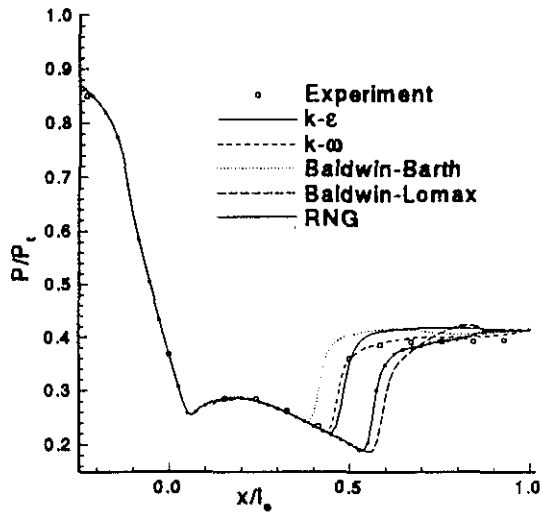


Figure 7. Surface pressure distributions (NPR=2.41).

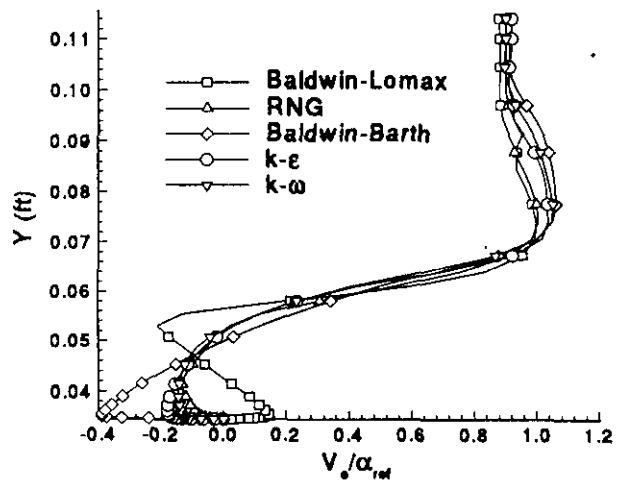


Figure 8. Exit velocity profiles (NPR=2.41)

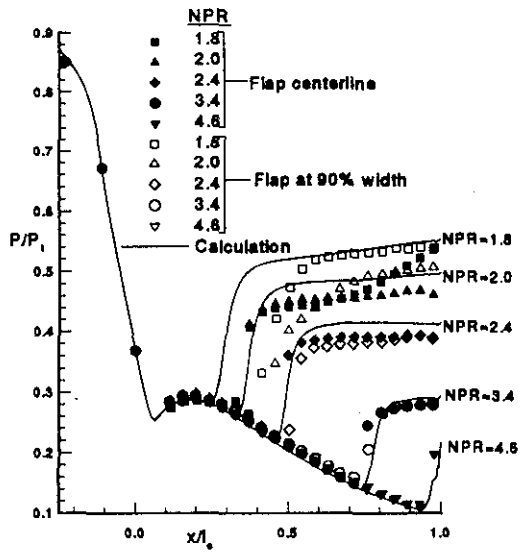


Figure 9. Surface pressure distribution using Chien's $k-\epsilon$ turbulence model

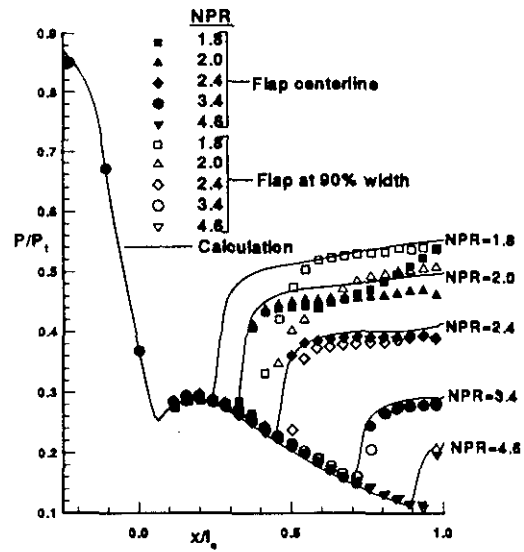


Figure 10 Surface pressure distribution using Wilcox's $k-\omega$ turbulence model.

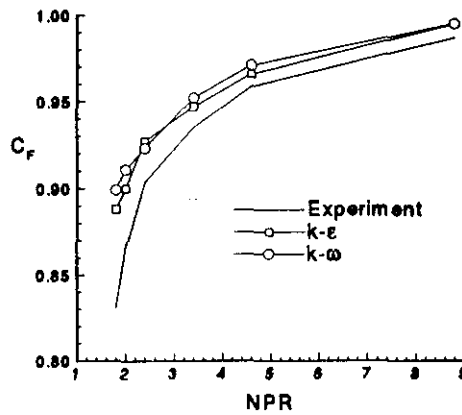


Figure 11 Thrust coefficient predictions